SSRG International Journal of Electrical and Electronics Engineering
ISSN: 2348-8379/ https://doi.org/10.14445/23488379/IJEEE-V11I11P133

Volume 11 Issue 11, 349-359, November 2024


*Original Article*

# Optical Design of Low Beam Headlight and Channel Modelling for Visible Light Vehicular Communication

Charu Priya S[1], Deepa T[1]*, Shih-Hsin Ma[2], Po-Sung Huang[2], Cheng-Hung Tsai[2]

[1]*Department of Electronics and Communication Engineering, SRM Institute of Science & Technology, Tamil Nadu, India.*
[2] *Department of Photonics, Feng Chia University, Seatwen, Taichung City, Taiwan, ROC.*

**Corresponding Auhtor : deepat@srmist.edu.in*

Received: 18 September 2024 Revised: 19 October 2024 Accepted: 17 November 2024 Published: 30 November 2024

***Abstract -*** *The motivation for Vehicular Visible Light Communication (VVLC) is the demand for automotive communication and the restricted bandwidth of Radio Frequency (RF) systems. VLC is a potential possibility for Vehicle-to-Vehicle (V2V) and Vehicle-to-Infrastructure (V2I) Connectivity due to the wide use of Light-Emitting Diodes (LEDs). Within this work, a novel low-beam headlamp designed adheres to the ECE R112 standard. The proposed design comprises the LED, ellipsoid reflector, mirror, baffle, and lens from which the optical path and power are determined with the help of non-sequential ray tracing. After importing this data into MATLAB, the relevant Channel Impulse Response (CIR) and accurate path loss are determined. The total luminous intensity from the proposed headlamp is 308.5 lm, and the overall effectiveness is 56.13%. This non-sequential ray tracing result is analyzed in comparison with the path loss model proposed and a linear model. The proposed path loss obtained for this headlamp is -56 dB, approximately 14 dB less than the Lambertian model.*

***Keywords -*** *Channel impulse response, Channel modelling, Low-beam headlamp, Optical wireless communication, Path loss, Vehicular communication, Visible light communication.*

## 1. Introduction

Light-Emitting Diodes (LEDs) are used in the automobile's headlamps, rear lamps, stop lamps, direction indicators, fog lamps, and daytime running lights. They enhance lighting efficiency and increase design flexibility and cost savings [1]. Applications for the vehicular network are categorized into those that are safety-related and those that are not [2, 3]. Automobile applications need seamless connectivity with high reliability, low latency, and effective data rates [4, 5]. A performance comparison between Visible Light Communication (VLC) and Radio Frequency (RF) was provided in [6]. VLC is more advantageous than RF. However, there are limitations, such as ambient noise and visibility limiters like fog in outdoor VLC [1]. Background noise interference and overcast conditions challenge the usage of VLC in vehicular communication. Hence, a flexible channel model and a robust optical design are necessary.

VLC and RF hybrid systems improve dependability and performance. The decode-forward hybrid cognitive VLC/RF system uses a binary architecture with both a direct link and a decode-forward link to swap between VLC and RF [7]. The authors in [8] studied the vehicle-streetlight VLC link to analyze the SNR degradation by integrating the solar irradiance model and asymmetric radiation using non-sequential ray tracing. Thus, it highlights the need for advanced noise mitigation techniques for outdoor VLC systems. The complex performance and power needs have made vehicular communication increasingly tense [9]. discussed techniques like multi-camera receiver array and optical backscatter decoding to meet the distinct requirements of vehicular networks. The mitigation of noise interference in different domains is discussed [10]. Electronic circuits isolate the DC components to reduce ambient light interference, polarization filters dismiss unpolarised light, composite LED robust communication, and higher modulation improve reliability against noise.

Precise characterization of the illumination is critical in Vehicular VLC (VVLC) [11-13]. According to ECE R112, the optic low-beam headlamp's design should ensure that the illumination source's beams generate the prescribed pattern [14]. The multi-module headlamp with non-symmetric floorboard and horizontal floorboard was developed [15]. A low-beam model built on a microlens array was presented [16]. A concept for low-beam lighting using a single bright LED with a non-spherical reflector and lenses was presented [17]. The prism and filter structure were altered to adjust the observed pattern. Two ellipsoidal reflectors producing low and high beam patterns, forming the compound reflector, are given [18]. Furthermore, an Achromatic LED Projection Headlamp (ALPH) with an achromatic doublet was used to

compensate for color dispersion [19]. These designs comply with ECE R112 for low-beam design. However, they do not consign to the VVLC demands, especially for communication-centered channel modelling and performance.

LEDs emit a Lambertian light. However, the headlamp optics' refractions and internal reflections determine the final pattern. Ray tracing is a geometric deterministic model for simulating the illumination pattern and the vehicular channel, which needs an explanation of the propagation environment [20-22]. The empirical observations with ray tracing in three transmission situations are studied [23]. A statistical channel model was proposed, including non-line-of-sight components and differences in vehicle separation, traffic flow, and channel geometry on transmission loss [24]. Three different taillights were used to measure the radiation and obtain the channel response [25]. The error probability is derived using Gaussian approximation [26]. Most existing models overlook the impact of path loss due to asymmetrical illumination. The novelty of this study lies in a low-beam headlamp that not only complies with the ECE R112 standard but also caters specifically to VVLC applications by integrating non-sequential ray tracing for precise optical modelling and channel characterization. Unlike others, this work incorporates the unsymmetrical pattern into a committed path loss model and demonstrates meaningful performance improvements. The main contributions are:

- To design a low-beam headlamp against the ECE R112 standard, integrate non-sequential ray tracing in path loss to account for unsymmetric illumination, and address the constraints of Lambertian and analytical models.
- To validate measurable improvements in transmission distance and efficiency under varying weather conditions compared to existing path loss models.

Hence, an allied approach is needed to address the gaps and integrate the headlamp design, channel model, and performance analysis. Section 2 gives the ECE R112-compliant headlamp design. Section 3 depicts the proposed VVLC channel model. Section 4 discusses the performance metrics. The results are discussed in Section 5. The future works and conclusion are given in Sections 6 and 7.

## 2. Design of Low-Beam Headlight

### *2.1. Requirements of Headlamp Illumination Profile*

The central aspect of a low-beam light is that it should not dazzle the approaching users while providing adequate light [14]. The headlamp's radiant region should cover a distance of about 25 to 50 m. The illumination must have a distinct boundary in a non-axisymmetric luminous distribution and should comply with the ECE R112 standard. The target plane is separated into illumination regions and measurement points. The headlamp is aimed at a vertical screen at a 25 m distance. According to the spherical coordinate measuring system, h-h is the horizontal plane, and v-v is the perpendicular plane to the polar axis (see Figure 1).

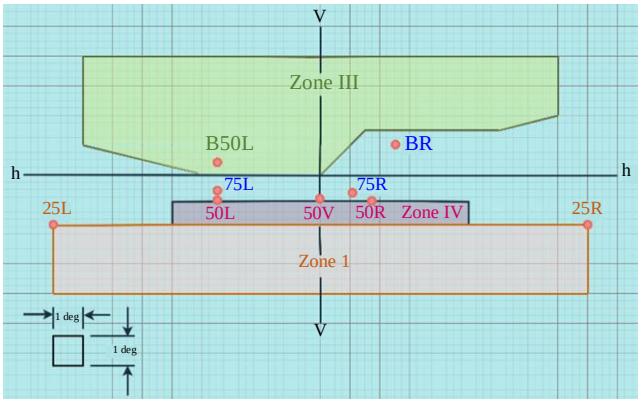


**Fig. 1 Illumination pattern as per the regulation of ECE R112**

Each grid in the illumination pattern corresponds to a 1° variation of the axes. This projection screen plots the luminous intensity and the angle between the origin (h-v) and the illuminating beam. The elevation angle ($\Theta$) determines the spread of the beam to the sides. The azimuth angle ($\Phi$) affects the length of the illuminated area in front of the lamp. There are 9 test points: 25R, 25L, 50R, 50L, 50V, 75R, 75L, B50L, and BR, and four zones: zone I, zone II, zone III, and zone IV. Each point in the zone I must have a maximum intensity of 2·ι, where ι is the intensity at 50R or 50L. The values should not exceed 625 cd in zone III. Zone IV should have a minimum intensity of 2500 cd.

### *2.2. LED Light Source*

The five-chip OSRAM OSLON® Black Flat KW H5L531.TE LED is employed as the light source [27]. It can provide bright ultra-white light while consuming little power, with an efficiency of up to 130 lm/W. This LED is said to be a Lambertian emitter. Before building the headlamp, the LED must be examined and tested for Lambertian emission and spectral distribution. For measuring light intensity emitted, the LED is mounted on a motorized rotating stage (see Figure 2).

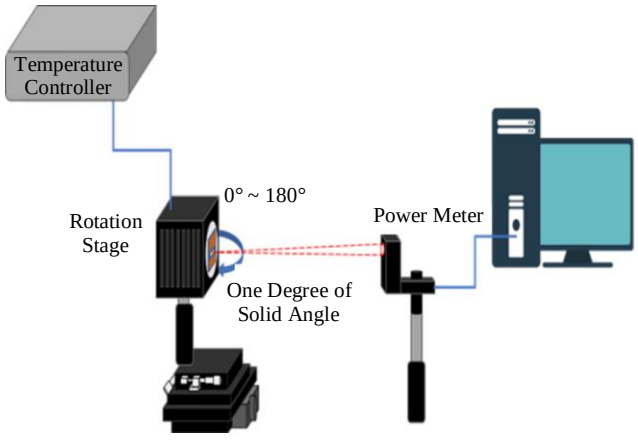


**Fig. 2 Experimental setup to measure luminous intensity**

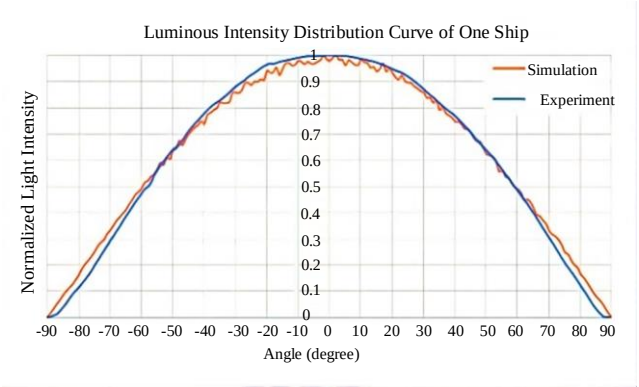


**Fig. 3 Intensity distribution curve of one chip LED**

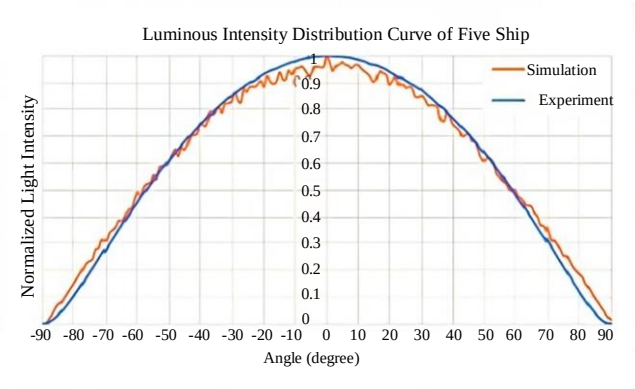


**Fig. 4 Intensity distribution curve of five chips LED**

This rotates the LED by one degree of solid angle, and the power meter measures the corresponding intensity. Figure 3 and Figure 4 show the intensity distribution of the LED with one chip and five chips. The simulated and experimental findings coincide. Thus, the LED is Lambertian.

The spectral flux measurement setup comprises an integrating sphere and a spectrum meter (see Figure 5). The integrating sphere is a hollow spherical chamber with a reflective surface to diffuse light. The spectrum meter placed at one end measures the light emitted by the LED at the other end inside the sphere. If λ is the wavelength of the light emitted, and F is the source's radiant flux, the measured spectral flux coincides with the theoretical value given by $I(\lambda) = F/(\Delta\lambda)$. Figure 6 shows this LED can provide a visible light spectrum from 380 nm to 790 nm.

### *2.3. Design of Low-Beam Headlamp*

The radiation is spread on the measuring plane 25 m from the luminaire. The following elements are used: outer hemispherical baffle, quarter ellipsoidal mirror, boundary baffle, angled mirror, and lens. The outer hemispherical baffle encloses the whole headlamp structure and absorbs the beams that do not pass through the lens. The quarter ellipsoidal mirror is curved to reflect the light in one direction and prevent excessive glare. The LED is positioned in the first focus of the ellipsoidal mirror. The proposed low-beam headlamp's schematic diagram and internal structure with dimensions are given in Figure 7 and Figure 8, respectively. The position of the five-chip LED inside the ellipsoidal reflector is shown in Figure 9. The rays from the LED are reflected inside the mirror and pass through the boundary baffle at the second focus. Table 1 contains the specifications for the proposed headlamp design.

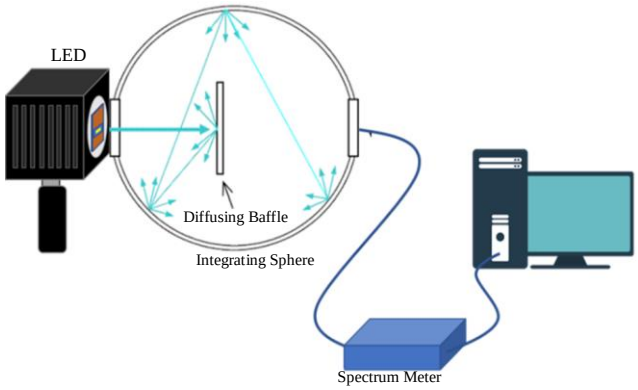


**Fig. 5 Experimental setup to measure the spectral flux**

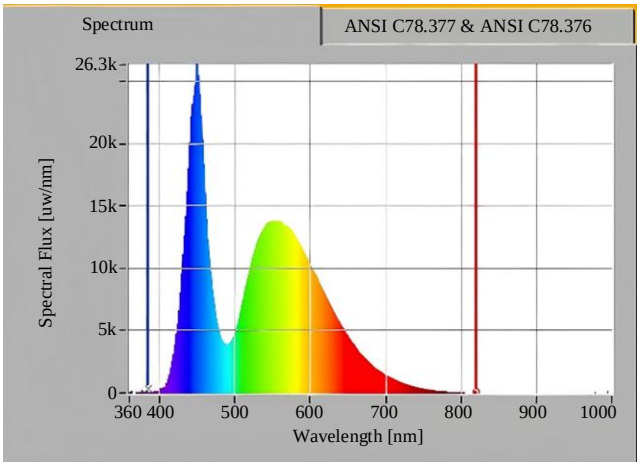


**Fig. 6 Spectrum distribution obtained for the LED**

**Table 1. Specifications of the headlamp design**

| Parameters | Values |
|---|---|
| Hemispherical Baffle | |
| **Radius** | 250 mm |
| Quarter Ellipsoidal Mirror | |
| **Short Axis Radius** | 45 mm |
| **Long Axis Radius** | 63.4 mm |
| **Distance between Focal Points** | 89.6 mm |
| **First Focal Point at** | 18.6 mm |
| **Reflectance** | 90% |
| Angled Mirror | |
| **Length** | 90 mm |

| | |
|---|---|
| **Width** | 25 mm |
| **Reflectance** | 90% |
| Boundary Baffle | |
| **Length** | 90 mm |
| **Height** | 50 mm |
| **Reflectance** | 0% |
| Lens | |
| **Focal Length** | 68.8 mm |
| **Aperture** | 70 mm |
| **Conic Constant (Surface 1)** | -302.385 |
| **Radius of Curvature (Surface 1)** | 325.979 |
| **Conic Constant (Surface 2)** | -0.421 |
| **Radius of Curvature (Surface 2)** | -40.214 |

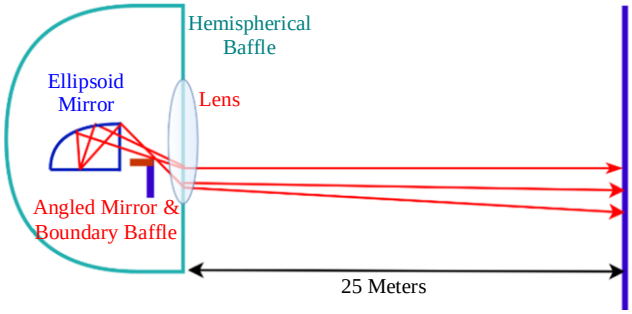


**Fig. 7 Schematic diagram of the proposed headlamp**

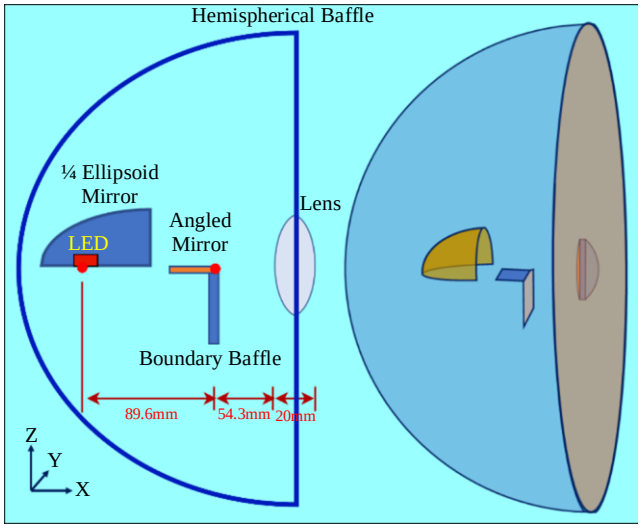


**Fig. 8 Internal structure of the proposed headlamp**

The boundary baffle comprises light-absorbing material to block the light that would be projected above the cut-off line. Hence, a clear cut-off line is produced according to ECE R112. The angled mirror mounted over the boundary baffle effectively uses the emitted light by redirecting any scattered or stray light toward the lens.

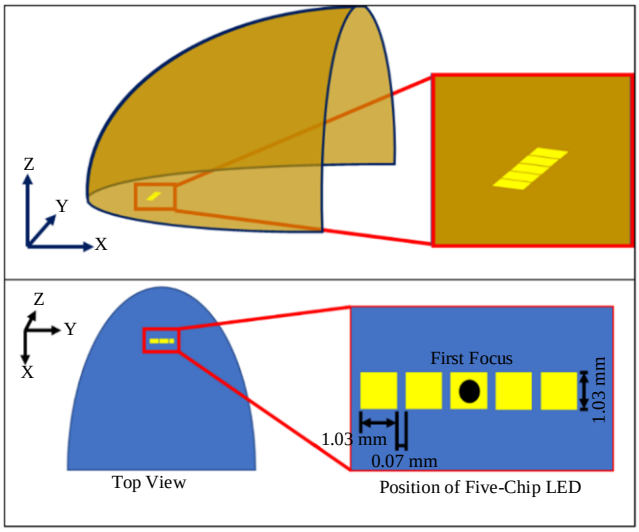


**Fig. 9 Position of LED in the quarter ellipsoid reflector**

This ensures that a significant portion of the light output is efficiently projected forward, improving road illumination while minimizing wasted light and enhancing overall efficiency. The overall length of the angled mirror is 90 mm, and an inclination of 15° is given at the mirror's center, as shown in Figure 10. Also, the mirror area of 0.2 mm width is removed at the center. The reflectance of this mirror is 90%. Placed in front of the headlamp, the lens is responsible for distributing and shaping the light emitted by the headlamp. It works in conjunction with other components. The lens is engineered with two surfaces to meet regulatory requirements and ensure efficient lighting performance. It has a semi-diameter of 31.02 mm.

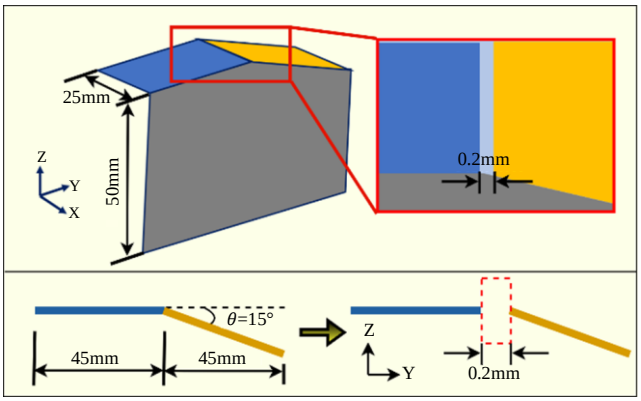


**Fig. 10 Dimensions of angled mirror and boundary baffle**

**Table 2. Simulation parameters**

| **Parameters** | **Values** |
|---|---|
| Transmitter | |
| **Type** | Low-beam headlamp |
| **LED** | Black Flat KW H5L531.TE |
| **Power ($P_T$)** | 1 W |

| Receiver | |
|---|---|
| **Type** | Photodiode |
| **Area ($A_P$)** | 1 $cm^2$ |
| **FoV** | 180° |
| **Responsivity ($R_{PD}$)** | 0.54 A/W |
| **Noise PSD ($N_{tot}$)** | $10^{-21}$ W/Hz |
| Road | |
| **Type** | R2 (Asphalt with 60% Gravel) |
| **Reflectance** | Q = 0.07, S = 0.582 |
| Weather (Clear weather) | |
| **Particle Index** | 1.000277 |
| **Size** | $10^{-4}$ |
| **Extinction Coefficient** | $1.5 \cdot 10^{-5}$ |
| Weather (Rain) | |
| **Particle Index** | 1.3 |
| **Size** | 100 |
| **Extinction Coefficient** | $0.9 \cdot 10^{-5}$ |
| Weather (Fog) | |
| **Particle Index** | 1.3 |
| **Size** | 10 |
| **Extinction Coefficient** | 0.00782 |

## 3. Vehicular VLC Channel Modelling

Considering a V2V situation, one vehicle communicates with another with the proposed headlamp as the transmitter. The Photodetector (PD) at the rear of another is the receiver. The Channel Impulse Response (CIR) incorporates attenuation loss and geometric path loss. The received radiation comprises Line-of-Sight (LOS) and Non-LOS (NLOS) components that vary by distance, incident angle, road surface, and weather. The road surfaces are classified by the average luminance coefficient (Q) and specular factor (S) by the International Commission on Illumination [28]. Here, the R2 surface (mixed diffuse and specular) and three weathers are considered. Clear and rainy conditions do not attenuate the light to a great extent since the attenuation is nearly zero. Fog is the major scattering element because its size is similar to the light wavelength [28].

### *3.1. Lambertian Modelling Approach*

The Lambertian model is commonly used to compute CIR. The distance (*D)*, power, and the receiver's orientation determine the received signal strength. *m* is the order of Lambertian emission, φ, and Ω are the irradiance and incidence angles. If φ = Ω, the Lambertian path loss is:

$$P_l = 10log_{10}\big(A_P(m+1)\big) - 10log_{10}(2\pi) - 20log_{10}(D) + 10(m+1)log_{10}(\cos(\varphi)) \quad (1)$$

If the vehicles are aligned in the same queue, then φ = Ω = 0.

$$P_l = 10log_{10}\big(A_P(m+1)\big) - 10log_{10}(2\pi) - 20log_{10}(D) \quad (2)$$

### *3.2. Ray Tracing Modelling Approach*

Though the LED emits light in a Lambertian pattern, the final unsymmetrical pattern depends on the headlamp optics. So, employing the classic Lambertian model, which has gained widespread use in indoor VLC, is impossible [29]. Non-sequential ray tracing is used in optical design to mimic light propagation through a system that includes non-ideal components based on Monte Carlo ray tracing. Each ray is traced as it interacts with optical elements, undergoing refraction, reflection, or absorption. It is used to accurately model the unsymmetric lighting of the low-beam headlamp and the channel model in varying environments.

The Black Flat KW H5L531.TE LED source was modelled as a Lambertian emitter with a normalized power of 1 W and a spectral range of 400–700 nm. As mentioned in section 2.3, the low-beam headlamp is designed using this LED as the transmitter. A 180° FoV receiver with a responsivity of 0.54 A/W and an area of 1 $cm^2$ is used. Road surface reflectance and weather conditions (clear, rain, fog) were included to replicate realistic scenarios. All the ray-tracing parameters are given in Table 2. Non-sequential ray tracing was preferred because it can precisely simulate intricate optical designs. It allows for modelling adverse weather like rain, fog, dust, and snow and accounts for attenuation, scattering, and absorption. It also allows the designers to evaluate how different angles affect the signal and optimize the system accordingly. Hence, it is ideal for modelling the headlamp optics and varying channel characteristics due to different environmental conditions.

The ray tracing involves the following steps [25]. The positions and shapes of all the optical elements specify the geometry of the optical system. Then, initial rays are generated to simulate the system's light behavior. These rays are traced through the optical system as they interact with various optical elements. The position and direction of each ray are updated along the optical path. Finally, the power and delay of each ray are calculated. Then, the CIR is computed by importing these ray-tracing results into MATLAB [24]. Figure 11 depicts the block diagram of the VVLC system.

CIR describes the channel's timely behavior in response to a short-time optical pulse. If x(t) is transmitted, then y(t) received is given as a convolution of x(t) and CIR [30]. When the ray tracing data have been loaded into MATLAB, the CIR is as follows:

$$h_{RT}(t) = \sum_{j=1}^{p} P_j\, \delta(t - \tau_j) \quad (3)$$

Where 'p' is the number of rays. $\tau_j$ and $P_j$ are the delay and power of the $j^{th}$ ray [31]. δ is the Dirac Delta function. The time spread and dispersion, path loss, and channel DC gain are obtained from the CIR. The channel DC gain is: [32]

$$H_0 = \int_{-\infty}^{\infty} h(t)\, dt \tag{4}$$

The difference between transmitted power ($P_{trans}$) and path loss ($P_l$) yields the total received power ($P_{rec}$). Hence, the received power is based on transmitted power, antenna gain, operating frequency, and distance. The path loss is: [25]

$$P_l = 10\, log_{10}\left[\int_0^{\infty} h(t)\, dt\right] \tag{5}$$

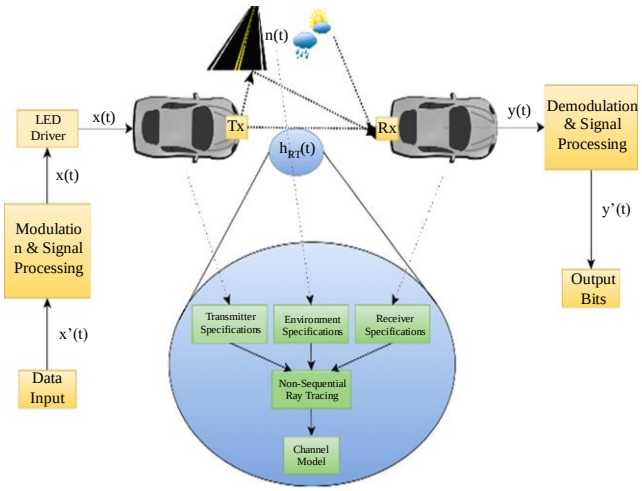


**Fig. 11 Block diagram of proposed VVLC system**

The Root Mean Square (RMS) delay spread quantifies the periodic scatter of the power delay. A high RMS delay implies higher time dispersion, resulting in inter-symbol interference and reduced Signal-to-Noise Ratio (SNR). The RMS delay spread ($\tau_{Rms}$) and the mean excess delay ($\alpha_0$) are:

$$\tau_{Rms} = \left[\frac{\int_0^{\infty}(t-\alpha_0)^2 h^2(t)\, dt}{\int_0^{\infty} h^2(t)\, dt}\right]^{1/2} \tag{6}$$

$$\alpha_0 = \frac{\int_0^{\infty} t\,.\, h^2(t)\, dt}{\int_0^{\infty} h^2(t)\, dt} \tag{7}$$

### *3.3. Path Loss Expression*

Attenuation due to environmental extinction and geometrical loss due to transmitter-receiver distance is:

$$P_{la} = \exp(-\gamma D) \tag{8}$$

$$P_{lg} = \frac{1}{D^{2\beta}} \cdot A_P \cdot I(h,v) \tag{9}$$

γ is the extinction coefficient, I(h,v) is the intensity distribution obtained from ray tracing, and β is the degradation factor. I(h,v) is a function of the horizontal spread angle $\Theta$, vertical angle $\Phi$, and incident angle ϕ. Thus, the total received power is given by the expression:

$$P_{rec} = P_{trans} P_{la} P_{lg} \tag{10}$$

$$P_{rec} = P_{trans} \cdot D^{-2\beta} \cdot A_P \cdot I(h,v) \cdot \exp(-\gamma D) \tag{11}$$

The path loss is the ratio of the transmitted power to the received power. Hence, the proposed ray tracing-based path loss for the VVLC system is:

$$P_L(D) = P_L(0) - 20\beta log_{10}(D) + 10log_{10}\big(A_P \cdot I(h,v)\big) - 10\frac{\gamma D}{\ln(10)} \tag{12}$$

The ray tracing simulation determines the value of β for each weather condition. $P_L(0)$ is the path loss reference taken at a 1 m distance. Also, the linear closed-form path loss expression of [33] is used for comparison. The values of $\rho$ and $\xi$ are obtained using data fitting.

$$P_{linear} = \rho D + \xi, D \geq 10\, m \tag{13}$$

## 4. Performance of VVLC system

The Non-Return to Zero (NRZ) on-off keying (OOK) modulation represents digital data with on or off levels. It shows minimal susceptibility to some noise and provides enough capacity for short-range VVLC applications. $x'_{OOK}(t)$ is the input data, $A_t$ is the carrier amplitude, and f is the carrier frequency. The modulation, received signal, and demodulation expressions for the VVLC system are:

$$x_{OOK}(t) = x'_{OOK}(t)[A_t \cdot \cos(2\pi f t)] \tag{14}$$

$$y(t) = x_{OOK}(t) \otimes h_{RT}(t) + n(t) \tag{15}$$

$$y'_{OOK}(t) = \begin{cases} 1, if\ y(t) \geq T_h \\ 0, if\ y(t) < T_h \end{cases} \tag{16}$$

The OOK demodulation is given by the threshold level ($T_h$). Besides the signal-induced shot and thermal noise, the VVLC system suffers from ambient light-induced noise. $B_n$ is the noise bandwidth, $N_{SH\text{-}s}$ is the signal-induced noise Power Spectral Density (PSD), $N_{SH\text{-}b}$ is the ambient noise PSD, and $N_{TH}$ is the thermal noise PSD. Then, the total noise PSD is:

$$N_{Tot} = N_{SH-s} + N_{SH-b} + N_{TH} \tag{17}$$

$H_0(D)$ represents the DC gain of the channel at D, ρ is the electrical-optical conversion, then SNR and BER are: [32]

$$SNR(D) = \frac{[\rho R_{PD} H_0(D)]^2 P_T}{N_{Tot} B_n} \tag{18}$$

$$BER(D) = \frac{1}{2} erfc\left(\frac{\sqrt{SNR(D)}}{2\sqrt{2}}\right) \quad (19)$$

## 5. Results and Discussion

### *5.1. Low-Beam Headlamp Design Results*

The axes measurements in Figure 12 are given as sin θ. θ corresponds to -9° to 9° angles in both the axes. The compliance of the proposed low-beam headlamp with ECE R112 was checked by measuring the illumination at individual test points and zones. The luminous intensity at each point was compared to the required values outlined in the standard, ensuring that the intensity in each point in Zone I was ≤ 2·ι and in Zone III was ≤ 625 cd. The blue points symbolize that the luminescence measurements are greatly preferable to those specified by the guidelines (see Figure 12).

The green and yellow points refer to the measurements that fulfill and those that hardly fulfill the guidelines. Table 3 compares the regulation and the proposed results. Figure 13 shows the directivity pattern that was obtained. The total lumens obtained by non-sequential ray tracing is 308.5 lm. The optical efficiency of a lighting system is computed by the output luminous flux measured across all test points with respect to the flux emitted by the source. The efficacy of the proposed low-beam headlamp is 56.13%.

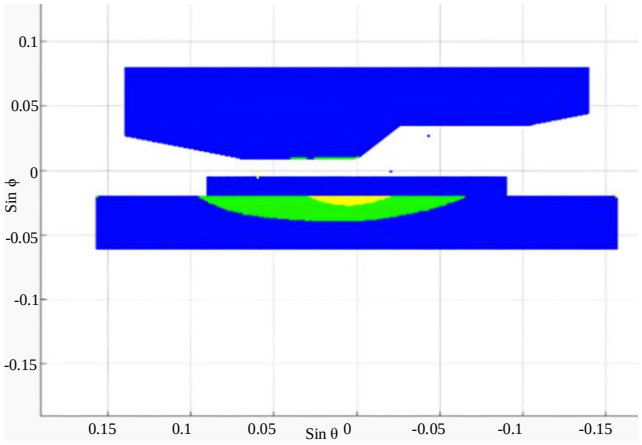


**Fig. 12 The illumination pattern compliance with regulation**

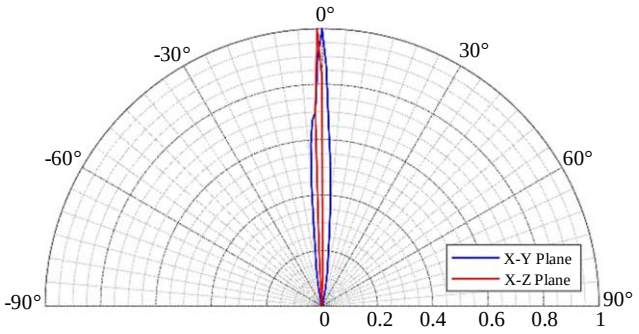


**Fig. 13 Measured radiation pattern of proposed low-beam headlamp**

**Table 3. Comparison of measured illuminance with ECE R112**

| Test Points | Regulation (cd) | Simulation (cd) |
|---|---|---|
| **25R** | ≥ 1700 | 1701.96 |
| **25L** | ≥ 1700 | 2784 |
| **50R** | ≥ 10100 | 21434.6 |
| **50L** | ≤ 13200 | 12865.8 |
| **50V** | ≥ 5100 | 27857.3 |
| **75R** | ≥ 10100 | 23904.8 |
| **75L** | ≤ 10600 | 9299.64 |
| **BR** | ≤ 1750 | 0 |
| **B50L** | ≤ 350 | 0 |
| **Zone I** | ≤ 2·ι | Pass |
| **Zone III** | ≤ 625 | Pass |
| **Zone IV** | ≥ 2500 | Pass |

The proposed design is more efficient than the earlier (e.g., [16, 17]) low-beam designs with microlens arrays and non-spherical reflectors by using efficient and simple optical components and better compliance with the ECE R112 standard. This results in a 14 dB reduction in path loss compared to the Lambertian model.

**Table 4. Channel parameters' values**

| Parameters | Clear Weather | Rain | Fog |
|---|---|---|---|
| **$\alpha_0$ (ns)** | 84.34 | 84.36 | 84.40 |
| **$\tau_{RMS}$ (ns)** | 1.22 | 1.24 | 1.27 |
| **$H_0$** | 2.46e-6 | 1.94e-6 | 1.07e-6 |
| **$P_l$ (dB)** | 56.0906 | 57.1219 | 59.6899 |

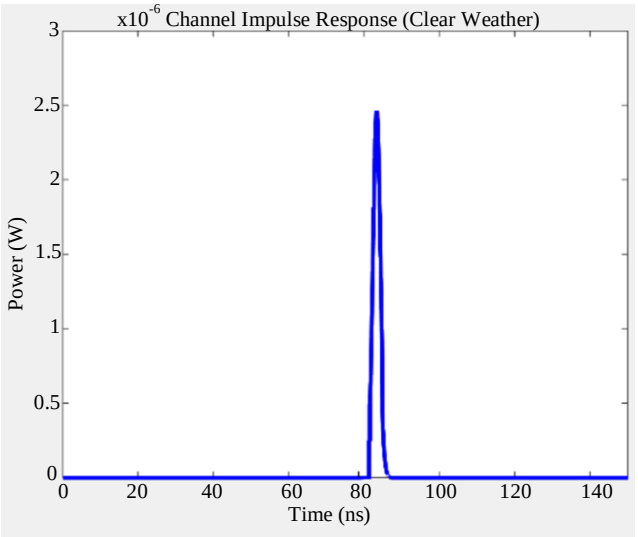


**Fig. 14 CIR at 25m distance for clear weather**

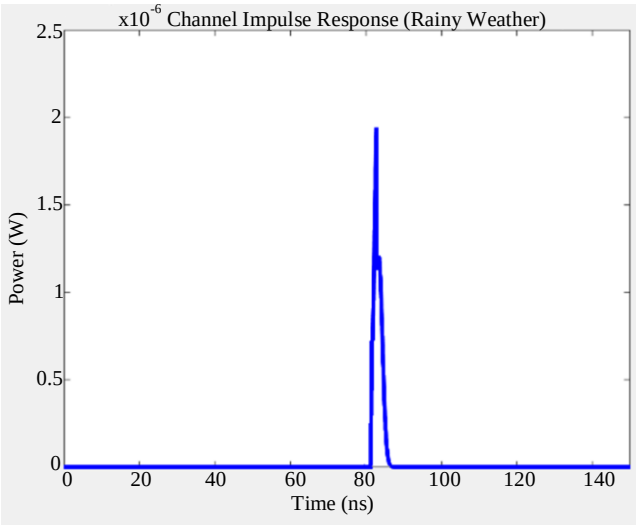


**Fig. 15 CIR at 25m distance for rainy weather**

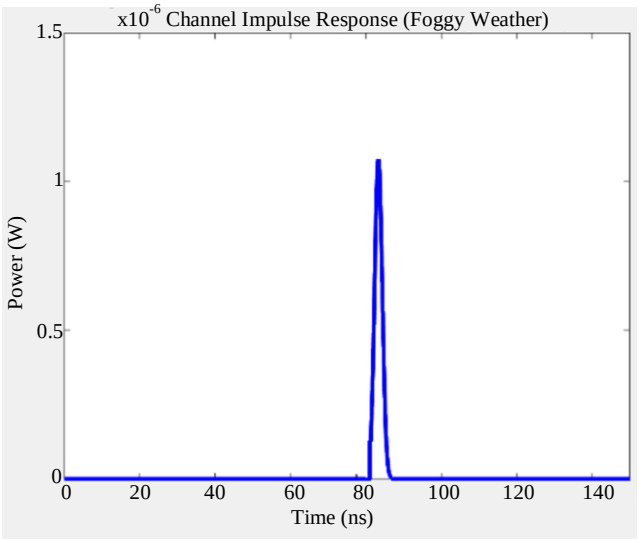


**Fig. 16 CIR at 25m distance at Fog**

### *5.2. Channel Modelling Results*

The peak power of CIR in clear weather is 2.46e-6 W, which is the maximum received power after traveling through the channel. The peak power occurs at 83.40 ns, indicating the arrival time of the straight path from transmitter to receiver. The sharp, concentrated peak implies high signal integrity in clear conditions. The CIR amplitude in rain (1.94e-6 W) is 80% of that in clear weather (see Figures 14, 15). The specular reflectance causes higher attenuation due to the signal reflected away from the receiver. After the main peak, there is a slight dip and additional small peaks. This secondary peak and ripples indicate multipath effects due to rain. Thus, delayed components in rainy conditions increased the RMS delay spread to 1.24 ns (see Table 4). The CIR in fog is 44% clear weather (see Figure 16). Though mixed diffuse and specular reflectance is considered, the gain is reduced because of the high fog. The CIR peak is narrower, indicating rapid attenuation and signal decay after the primary peak. Hence, the power dissipates with slight ripples and no visible secondary peaks. Unlike rain, where larger droplets can redirect light to form distinct multipath components, the scattering in fog is highly uniform and dispersive, effectively spreading the light in all directions without creating strong, separate paths. Thus, fog is a diffusive medium that blurs the light, leading to the highest path loss of -59.68 dB.

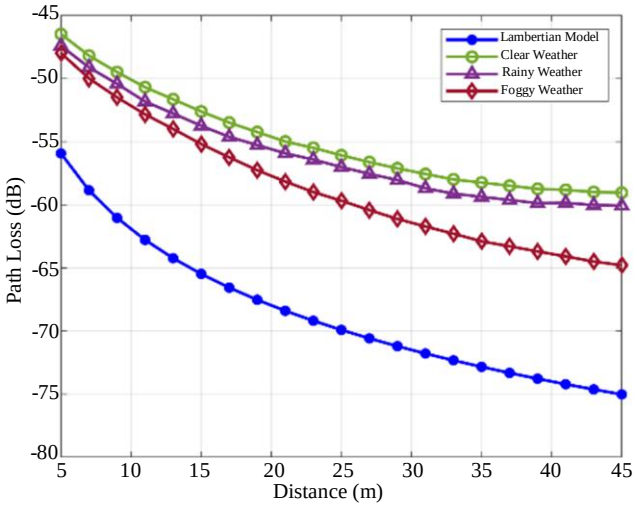


**Fig. 17 Path loss at Lambertian and different weathers**

### *5.3. Path Loss Results*

Figure 17 shows path loss for varying environmental situations. The proposed model's measured $P_L$ is -56 dB for clear weather, ~14 dB lower than the Lambertian model (-70 dB) at 25 m. The Lambertian model assumes an ideal isotropic emission pattern; light is radiated uniformly in all directions. However, the headlamp beam is focused in a particular direction, limiting geometric spreading, which leads to a lower path loss than the Lambertian model. The path loss obtained using the proposed model expression in Equation (12) is given in Figures 18, 19, and 20 for different weathers. It is seen that the proposed expression is perfectly analogous to the ray tracing. The value of β obtained using the ray tracing simulation is 0.71, 0.72, and 0.80 for clear, rainy, and foggy weather, respectively. The higher deterioration values in rain and fog indicate additional losses. Thus, models incorporating inverse-square law, exponential decay, and path loss exponents capture the VVLC attenuation behavior over varying distances.

The values of (ρ, ξ) of the linear model [33] are (-0.3862, -46.71), (-0.4071, -47.38), and (-0.4929, -47.68) for clear weather, rain, and fog. The baseline received power ξ decreases as the weather worsens, which is intuitive since fog and rain cause greater signal loss. However, the linear path loss model is applicable only for short distances since real-world situations vary over large distances.

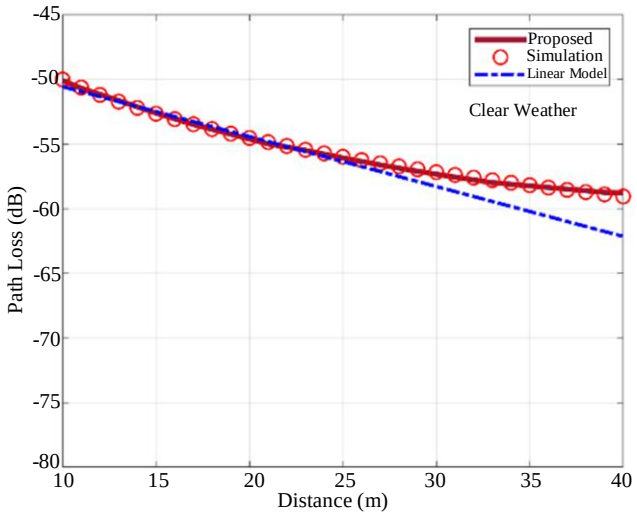


**Fig. 18 Comparison of path loss for clear weather**

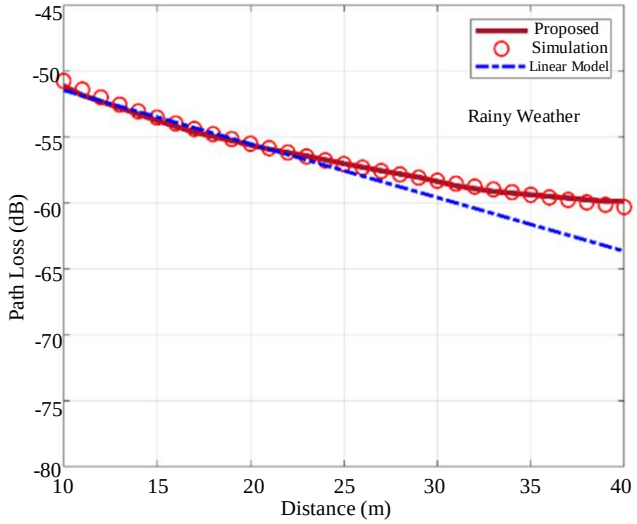


**Fig. 19 Comparison of path loss for rainy weather**

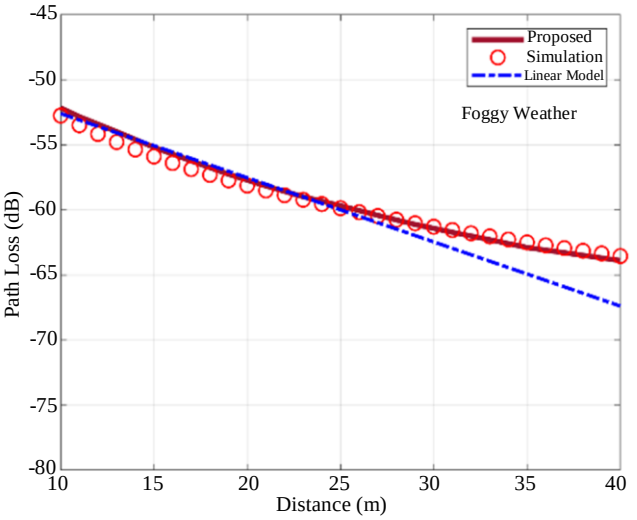


**Fig. 20 Comparison of path loss at Fog**

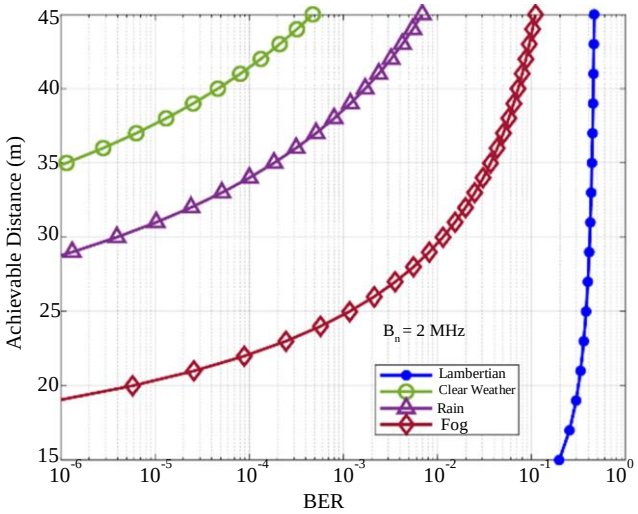


**Fig. 21 BER vs. distance for noise bandwidth of 2 MHz**

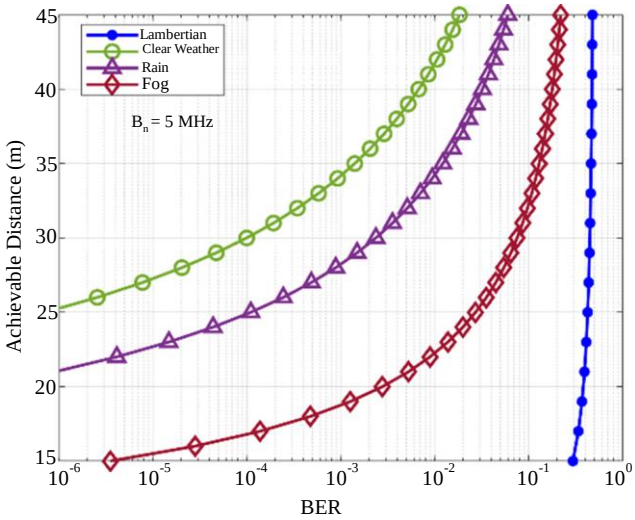


**Fig. 22 BER vs. distance for noise bandwidth of 5 MHz**

### *5.4. Link Performance Results*

Path loss increases as distance increases; BER is also high. When BER is $10^{-4}$, and bandwidth is $B_n$ = 5 MHz, achieved distances are ~29 m, ~25 m, and ~18 m for clear weather, rain, and fog (see Figure 22). For 2 MHz, ~45 m, ~31 m, and ~23 m (see Figure 21). The noise variance decreases when the bandwidth is reduced, thus improving SNR. Clear weather offers the maximum achievable distance for each BER due to minimal scattering compared to other conditions. Lambertian BER trends steeply down, showing that this model becomes ineffective as BER increases due to consideration of Lambertian emission. This proves the need to consider illumination patterns and environmental conditions when planning and deploying VVLC.

## 6. Future Work

This study focuses on simulation-based analysis to evaluate the proposed system. The characteristics of the

proposed VVLC system under a controlled environment are analyzed to optimize parameters before implementation. Real-time experimental validation is planned in the near future to assess the practical performance. The hybrid VLC/RF systems can strengthen both technologies. VLC can support robust, high-speed, secure data transmission in line-of-sight conditions and RF for non-line-of-sight conditions. Adaptive handling techniques between VLC and RF enable seamless connectivity in varying environmental conditions, such as fog or snow.

Global standardization provides the VVLC interoperability and connectivity between different manufacturers and infrastructures. The proposed system can be compared with alternative technologies like Dedicated Short-Range Communication (DSRC) and others to provide valuable insights into VVLC's pros and cons. It can also help identify scenarios where VVLC can provide high performance, such as low latency or highly secure data transfer. Adaptive filtering and machine learning-based predictions can mitigate interference due to high ambient noise levels. Channel coding techniques that minimize signal degradation should be enhanced to provide high data rates.

## 7. Conclusion

A low-beam headlamp design following ECE R112 regulation is built and analyzed. The channel model is used to compute the optical power values and delay obtained from non-sequential ray tracing. The total received lumens from the proposed headlamp is 308.5 lm, with an efficiency of 56.13%. When BER is $10^{-4}$, and noise bandwidth is 5 MHz, the system achieved transmission distances of 29 m in clear weather, 25 m in rainy conditions, and 18 m in fog. When the noise is reduced to 2 MHz, the distances improve to 45 m, 31 m, and 23 m respectively.

The proposed path loss model agrees with the simulation results from non-sequential ray tracing. These results underscore the robustness of the designed headlamp and ray tracing for VVLC applications, solidifying its potential for widespread adoption.

## References


[1] Nehad Hameed Hussein et al., "A Comprehensive Survey on Vehicular Networking: Communications, Applications, Challenges, and Upcoming Research Directions," *IEEE Access*, vol. 10, pp. 86127-86180, 2022. [CrossRef] [Google Scholar] [Publisher Link]

[2] Sharan H.S. et al., "Smart Vehicular Communication: A Survey," *International Journal of Engineering Research & Technology*, vol. 8, no. 15, pp. 146-151, 2020. [CrossRef] [Google Scholar] [Publisher Link]

[3] Dhaya Kanthavel, S.K.B. Sangeetha, and K.P. Keerthana, "An Empirical Study of Vehicle to Infrastructure Communications - An Intense Learning of Smart Infrastructure for Safety and Mobility," *International Journal of Intelligent Networks*, vol. 2, pp. 77-82, 2021. [CrossRef] [Google Scholar] [Publisher Link]

[4] M. Nadeem Ahangar et al., "A Survey of Autonomous Vehicles: Enabling Communication Technologies and Challenges," *Sensors*, vol. 21, no. 3, 2021. [CrossRef] [Google Scholar] [Publisher Link]

[5] M. Shunmugathammal et al., "Li-Fi Technology Based Automatic Vehicle Speed Controller," *2022 11th International Conference on System Modeling & Advancement in Research Trends (SMART)*, Moradabad, India, pp. 1084-1087, 2022. [CrossRef] [Google Scholar] [Publisher Link]

[6] Mehdi Karbalayghareh et al., "Channel Modeling and Performance Limits of Vehicular Visible Light Communication Systems," *IEEE Transactions on Vehicular Technology*, vol. 69, no. 7, pp. 6891-6901, 2020. [CrossRef] [Google Scholar] [Publisher Link]

[7] Eman Mohamed H. Abouzohri, and Mohamed M. Abdallah, "Performance of Hybrid Cognitive RF/VLC Systems in Vehicle-to-Vehicle Communications," *2020 IEEE International Conference on Informatics, IoT, and Enabling Technologies (ICIoT)*, Doha, Qatar, pp. 429-434, 2020. [CrossRef] [Google Scholar] [Publisher Link]

[8] Hossien B. Eldeeb, and Murat Uysal, "Visible Light Communication-Based Outdoor Broadcasting," *2021 17th International Symposium on Wireless Communication Systems (ISWCS)*, Berlin, Germany, pp. 1-6, 2021. [CrossRef] [Google Scholar] [Publisher Link]

[9] Lin Cheng et al., "Automotive Visible-Light Communication: Alternative Devices and Systems," *Tsinghua Science and Technology*, vol. 28, no. 4, pp. 719-728, 2023. [CrossRef] [Google Scholar] [Publisher Link]

[10] Moaaz Ahmed et al., "Multidomain Suppression of Ambient Light in Visible Light Communication Transceivers," *IEEE Transactions on Intelligent Transportation Systems*, vol. 23, no. 10, pp. 18145-18154, 2022. [CrossRef] [Google Scholar] [Publisher Link]

[11] Farshad Miramirkhani, and Murat Uysal, "Channel Modelling for Indoor Visible Light Communications," *Philosophical Transactions of the Royal Society A*, vol. 378, 2020. [CrossRef] [Google Scholar] [Publisher Link]

[12] Mohammed Salih Mohammed Gismalla et al., "Survey on Device to Device (D2D) Communication for 5GB/6G Networks: Concept, Applications, Challenges, and Future Directions," *IEEE Access*, vol. 10, pp. 30792-30821, 2022. [CrossRef] [Google Scholar] [Publisher Link]

[13] Hossien B. Eldeeb, Sadiq M. Sait, and Murat Uysal, "Visible Light Communication for Connected Vehicles: How to Achieve the Omnidirectional Coverage?," *IEEE Access*, vol. 9, pp. 103885-103905, 2021. [CrossRef] [Google Scholar] [Publisher Link]

[14] UNECE, Vehicle Regulations reg.112 rev.3, 2023. [Online]. Available: https://unece.org/transport/vehicle-regulations

[15] Chi-Chang Hsieh et al., "Design of Multi-Module Led Headlamp of Vehicle under Federal Motor Vehicle Safety Standard," *Sensors and Materials*, vol. 35, no. 7(3), pp. 2433-2448, 2023. [CrossRef] [Google Scholar] [Publisher Link]

[16] Hong Wang et al., "Design of a Newly Projected Light-Emitting Diode Low-Beam Headlamp Based on Microlenses," *Applied Optics*, vol. 54, no. 7, pp. 1794-1801, 2015. [CrossRef] [Google Scholar] [Publisher Link]

[17] Wen-Shing Sun et al., "Optical Design for a cost-Effective Low-Beam Headlamp with a White Light LED," *Optical and Quantum Electronics*, vol. 52, 2020. [CrossRef] [Google Scholar] [Publisher Link]

[18] Shang-Ping Ying et al., "Single Headlamp with Low-and High-Beam Light," *Photonics*, vol. 8, no. 2, 2021. [CrossRef] [Google Scholar] [Publisher Link]

[19] Shih-Hsin Ma, Chi-Hung Lee, and Chia-Hsian Yang, "Achromatic LED-Based Projection Lens Design for Automobile Headlamp," *Optik*, vol. 191, pp. 89-99, 2019. [CrossRef] [Google Scholar] [Publisher Link]

[20] Hossien B. Eldeeb et al., "Vehicular Visible Light Communications: The Impact of Taillight Radiation Pattern," *2020 IEEE Photonics Conference (IPC)*, Vancouver, BC, Canada, pp. 1-2, 2020. [CrossRef] [Google Scholar] [Publisher Link]

[21] Hossien B. Eldeeb et al., "Infrastructure-to-Vehicle Visible Light Communications: Channel Modelling and Performance Analysis," *IEEE Transactions on Vehicular Technology*, vol. 71, no. 3, pp. 2240-2250, 2022. [CrossRef] [Google Scholar] [Publisher Link]

[22] Wantanee Viriyasitavat et al., "Vehicular Communications: Survey and Challenges of Channel and Propagation Models," *IEEE Vehicular Technology Magazine*, vol. 10, no. 2, pp. 55-66, 2015. [CrossRef] [Google Scholar] [Publisher Link]

[23] Hossien B. Eldeeb et al., "Channel Modelling for Light Communications: Validation of Ray Tracing by Measurements," *2020 12th International Symposium on Communication Systems, Networks and Digital Signal Processing (CSNDSP)*, Porto, Portugal, pp. 1-6, 2020. [CrossRef] [Google Scholar] [Publisher Link]

[24] Farah Mahdi Alsalami et al., "Statistical Channel Modelling of Dynamic Vehicular Visible Light Communication System," *Vehicular Communications*, vol. 29, 2021. [CrossRef] [Google Scholar] [Publisher Link]

[25] Hossien B. Eldeeb et al., "Vehicular VLC: A Ray Tracing Study Based on Measured Radiation Patterns of Commercial Taillights," *IEEE Photonics Technology Letters*, vol. 33, no. 16, pp. 904-907, 2021. [CrossRef] [Google Scholar] [Publisher Link]

[26] Vipul Dixit, and Atul Kumar, "Performance Analysis of Non-Line of Sight Visible Light Communication Systems," *Optics Communications*, vol. 459, 2020. [CrossRef] [Google Scholar] [Publisher Link]

[27] OSRAM OSLON® Black Flat, KW H5L531.TE. [Online]. Available: https://ams-osram.com/products/leds/white-leds/osram-oslon-black-flat-kw-h5l531-te

[28] International Commission on Illumination (CIE), Vehicle Headlighting Systems Photometric Performance - Method of Assessment, 2011. [Online]. Available: https://cie.co.at/publications/vehicle-headlighting-systems-photometric-performance-method-assessment

[29] Farah Mahdi Alsalami et al., "Impact of Vehicle Headlights Radiation Pattern on Dynamic Vehicular VLC Channel," *Journal of Lightwave Technology*, vol. 39, no. 10, pp. 3162-3168, 2021. [CrossRef] [Google Scholar] [Publisher Link]

[30] Farah M. Alsalami et al., "The Statistical Temporal Properties of Vehicular Visible Light Communication Channel," *2020 12th International Symposium on Communication Systems, Networks and Digital Signal Processing (CSNDSP)*, Porto, Portugal, pp. 1-5, 2020. [CrossRef] [Google Scholar] [Publisher Link]

[31] Hisham Abuella et al., "ViLDAR-Visible Light Sensing-Based Speed Estimation Using Vehicle Headlamps," *IEEE Transactions on Vehicular Technology*, vol. 68, no. 11, pp. 10406-10417, 2019. [CrossRef] [Google Scholar] [Publisher Link]

[32] Hossien B. Eldeeb, Farshad Miramirkhani, and Murat Uysal, "A Path Loss Model for Vehicle-to-Vehicle Visible Light Communications," *2019 15th International Conference on Telecommunications (ConTEL)*, Graz, Austria, pp. 1-5, 2019. [CrossRef] [Google Scholar] [Publisher Link]

[33] Mohammed Elamassie et al., "Effect of Fog and Rain on the Performance of Vehicular Visible Light Communications," *2018 IEEE 87th Vehicular Technology Conference (VTC Spring)*, Porto, Portugal, pp. 1-6, 2018. [CrossRef] [Google Scholar] [Publisher Link]